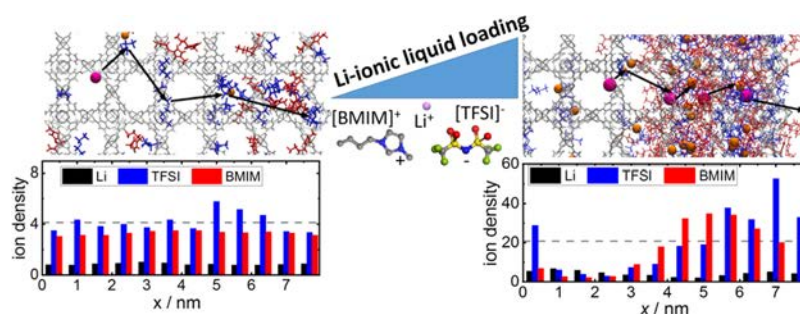


# Structural and Dynamic Insights into the Conduction of Lithium-Ionic-Liquid Mixtures in Nanoporous Metal–Organic Frameworks as Solid-State Electrolytes

Micaela Vazquez,<sup>‡</sup> Modan Liu,<sup>‡</sup> Zejun Zhang, Abhinav Chandresh, Anemar Bruno Kanj, Wolfgang Wenzel,<sup>\*</sup> and Lars Heinke<sup>\*</sup>



**ABSTRACT:** Metal–organic framework (MOF) based separators in Li ion batteries (LIBs) have the potential to improve the battery performance. The mobility and conduction of lithium and organic ionic liquids (ILs) in these materials acting as (quasi) solid state electrolytes are crucial for the battery power output. Here, we investigate the mobility of a Li based IL in MOF nanopores and unveil the details of the conduction mechanism by molecular dynamics (MD) simulations. A complex conductivity depending on the Li IL loading and on the IL composition is observed. Most importantly, the presence of Li prevents the collapse of the conductivity at high IL loadings. The fully atomistic MD simulations including guest–guest and guest–host interactions elucidate the competing mechanisms: Li follows a Grotthuss like conduction mechanism with large mobility. While at small pore fillings, the Li conduction is limited by the large distance between the anions facilitating the Grotthuss like conduction; the conduction at high pore fillings is governed by field induced concentration inhomogeneities. Because of the small MOF pore windows, which hinders the simultaneous passage of the large IL cations and anions in opposite directions, the IL shows field induced MOF pore blocking and ion bunching. The regions of low anion concentration and high cation concentration represent barriers for Li, decreasing its mobility. In comparison to Li free IL, the IL bunching effect is attenuated by the formation of charge neutral Li anion complexes, resulting in a tremendously increased conductivity at maximum pore filling. The exploitation of this mechanism may enhance the development of advanced batteries based on IL and nanoporous separators.

**KEYWORDS:** lithium conduction, ionic liquid, nanoporous materials, metal–organic frameworks, lithium ion batteries

## INTRODUCTION

Lithium ion batteries (LIBs) are the dominating energy storage units for portable electronic devices these days. In order to improve their safety, durability, power density, and applicable temperature range, new materials for electrolytes and separators are required.<sup>1,2</sup> Ionic liquids (ILs) are nonflammable, thermally stable molten salts of organic cationic and anionic molecules with negligible vapor pressure.<sup>3–6</sup> The application of ILs as electrolytes represents an environmentally friendly, durable, and safe alternative to the currently used organic solvents in LIBs.<sup>7,8</sup> In LIBs, but also in other batteries like lithium–sulfur and lithium–oxygen batteries or sodium ion batteries, IL electrolytes are embedded in nonconducting, porous separators, electronically isolating the anode and the cathode. The static and dynamic properties of liquids, ions, and

ILs under nanoconfinement in such porous hosts can be rather complex and may significantly deviate from the bulk properties.<sup>9–16</sup> For example, confining IL in subnanometer sized pores in porous carbon supercapacitors results in exceptionally high capacitances and energy densities.<sup>9,10</sup> The nanoconfinement may also result in the partial breaking of the Coulombic ordering.<sup>11</sup> The choice of the right separator in

battery materials is crucial, and the currently used materials need further improvement with respect to stability, durability, and ionic conduction.<sup>1</sup> Ideally, the separator material in batteries is a nonconducting porous solid with good physical properties, hindering Li dendrimer formations while protecting the electrodes from degradation. The separator should allow a high ionic conduction of the IL electrolyte and excellent IL wettability.

Metal–organic frameworks (MOFs) are a class of nano porous crystalline materials that have the potential to fulfill these requirements. MOFs are composed of organic di or multitopic ligand molecules connected by metal nodes, forming a three dimensional (3D) scaffold.<sup>17,18</sup> Their mechanical and physical properties make them suitable for a wide range of applications, and their structure can be tuned by appropriate choices of components.<sup>19–22</sup> MOFs, either pure or as fillers in composite polymer materials, are a very promising separator material and demonstrate the hindering of lithium dendrimer formation.<sup>23–25</sup> It was also demonstrated that MOFs can significantly stabilize the solid electrolyte interphase (SEI).<sup>26–29</sup> Moreover, using MOFs as separators increases the operative temperature range of batteries.<sup>23</sup>

A key feature of ILs@MOFs as (quasi) solid state electrolytes and of MOFs as separators is the ionic conductivity of the electrolyte in the pores. So far, in pioneering studies, the conduction of IL in the MOF material was determined for powders, typically pressed into pellets, by using electrochemical impedance spectroscopy (EIS).<sup>23,30–32</sup> For these MOF pellets, a significant amount of excess IL on the external MOF surface was reported,<sup>23,30,31</sup> which is also described as the “nanowetted interface”.<sup>30</sup> Because the mobility of the ions in the MOF tremendously decreases with confinement, the excess IL is typically much more mobile than the IL in the MOF pores. As result, the conductivity of the IL@MOF pellets measured by EIS may be dominated by the highly conducting excess IL, whereas the IL in the MOF pores barely contributes to the measured results. To investigate the IL mobility exclusively in the MOF pores, here, we use dense thin films of MOFs on a solid substrate, where excess IL can be washed off. It is important to note that the ion transport in the LIB separation layer is carried by the bulk material, this means in the pores of the MOF and not by the interfaces.

Here, we investigate the conduction and mobility of lithium based ionic liquids in well defined pores of crystalline MOFs. For precise conduction measurements, we use thin films of surface mounted metal–organic frameworks (SURMOFs) grown in a layer by layer (LbL) fashion on glass substrates with deposited interdigitated gold electrodes.<sup>33,34</sup> By rinsing the outer SURMOF surface, excess IL is removed from the surface of the dense films, leaving IL only in the pores of the nanoporous host. We investigate the conduction of the IL of type  $[\text{Li}_{0.2}\text{BMIM}_{0.8}][\text{TFSI}]$  in MOF films with the HKUST 1 structure and use  $[\text{BMIM}][\text{TFSI}]$  and Li TFSI in HKUST 1 as the reference systems. BMIM stands for 1 butyl 3 methyl imidazolium and TFSI denotes bis(trifluoromethylsulfonyl) amide, also referred to as  $\text{NTf}_2$ . Both ILs are popular prototype, aprotic ILs used in various energy related applications.<sup>35–37</sup> HKUST 1 has a rather rigid, face centered cubic structure with a unit cell size of 2.6 nm.<sup>3</sup> It has an isotropic 3d pore system with pores of approximately 1.3 nm diameter connected by pore windows (or pore apertures) of 0.9 nm.<sup>38</sup> The HKUST 1 SURMOF has good mechanical properties, such as a Young’s modulus of about 10 GPa<sup>19</sup> and

strong adhesion to the substrate.<sup>39</sup> Lithium loaded HKUST 1 demonstrated efficient ion conduction channels.<sup>40</sup> The utility and strong performance of HKUST 1 as separators<sup>41</sup> and cathodes<sup>42,43</sup> in lithium–sulfur batteries were demonstrated. We find that while the ion mobility and conduction of  $[\text{BMIM}][\text{TFSI}]$  in HKUST 1 tremendously decreases with increasing pore filling, as a result of mutual pore blocking by the large organic ions,<sup>44</sup> the conduction of  $[\text{Li}_{0.2}\text{BMIM}_{0.8}][\text{TFSI}]$  only slightly decreases with increasing pore filling. Molecular dynamics (MD) simulations, which qualitatively reproduce the experimental results, show that Li conduction follows a Grotthuss like mechanism, which, although Li represents only 10% of ions, contributes to 26 to 37% of the total conductivity. Two conduction regimes are unveiled: at low and medium concentrations, the Grotthuss like Li conduction is limited by the distance between the  $[\text{TFSI}]$  anions. At high loadings, the relatively large organic cations and anions show a field induced bunching and immobilization behavior, qualitatively similar to the Li free reference system. However, the formation of Li–TFSI cation–anion complexes, which are charge neutral and are not accelerated by the electric field, considerably decreases the bunching effect. As result, in comparison to the Li free IL, the ion bunching caused conduction collapse at full loading is prevented, and the conductivity at full loading is about two orders of magnitude larger.

## METHODS

**SURMOF Synthesis and Lithium and IL Loading.** SURMOF thin films were prepared in an LbL fashion.<sup>33,34</sup> In detail, the LbL synthesis consists in alternately exposing the substrate to the ethanolic solutions of the MOF building units, that is, the metal nodes, here, 0.5 mM copper acetate, as well as the organic linkers, here, 0.1 mM BTC (benzene 1,3,5 tricarboxylic acid). Between each immersion step, the samples were briefly cleaned with pure ethanol. The SURMOF samples were prepared in 50 LbL synthesis cycles using a dipping robot.<sup>45</sup> More details on the LbL SURMOF synthesis can be found in a previous study.<sup>33</sup> Before the SURMOF synthesis, the glass substrates with deposited interdigitated gold electrodes (IDE) were treated by the UV–ozone treatment for 30 min to remove impurities and to increase the number of OH functional groups and hydrophilicity. The IDE–glass substrates were obtained from DropSens. The gap width is 10  $\mu\text{m}$ . The total length of the gap between the gold electrodes is 1.69 m (= 2 times 125 gaps of 6.76 mm length).

The  $[\text{BMIM}][\text{TFSI}]$  IL and LiTFSI salt were purchased from Sigma Aldrich.  $[\text{Li}_{0.2}\text{BMIM}_{0.8}][\text{TFSI}]$  IL was prepared by mixing  $[\text{BMIM}][\text{TFSI}]$  and LiTFSI.

For both  $[\text{Li}_{0.2}\text{BMIM}_{0.8}][\text{TFSI}]$  and  $[\text{BMIM}][\text{TFSI}]$ , the IL loading of the HKUST 1 SURMOFs was performed by the immersion of the sample in IL:acetonitrile solutions with the IL ratios of 15, 50, 80, and 100%<sub>vol</sub>. After an immersion time of 20 min, the samples were briefly rinsed with acetonitrile for approximately 2 s to remove the IL from the outer sample surface; this means to remove the excess IL outside the MOF pores. Then, the samples were dried in a flow of pure nitrogen. The excess IL can be seen by the gloss; after rinsing off, the sample surface is matte.

The (reference) powder HKUST 1 sample was prepared by following the standard synthesis procedure.<sup>46</sup>  $\text{Cu}(\text{NO}_3)_2 \cdot 3\text{H}_2\text{O}$  (0.87 g, 3.6 mmol) and BTC (0.42 g, 2.0 mmol) were dissolved in 24 mL of 50:50 vol % mixture of ethanol and deionized water. The solution was kept in a Teflon lined stainless steel autoclave at 100 °C for 24 h. Upon cooling to room temperature, the powder was centrifuged and washed thoroughly with a mixture of water and ethanol (50% v/v). Finally, the powder was activated under vacuum at 120 °C for 16 h. Different amounts of  $[\text{Li}_{0.2}\text{BMIM}_{0.8}][\text{TFSI}]$  IL were added to the activated HKUST 1 powder separately, homogeneously mixed, and

heated under vacuum at 120 °C overnight. In detail, the IL amount was 66.47 mg of IL per 100 mg of MOF for 100% loading, 53.2 mg of IL per 100 mg of MOF for 80% loading, 33.2 mg of IL per 100 mg of MOF for 50% loading, and 9.9 mg of IL per 100 mg of MOF for 15% loading. These numbers of IL to MOF mass correspond to the numbers determined and shown in Figure 1c. For the preparation of

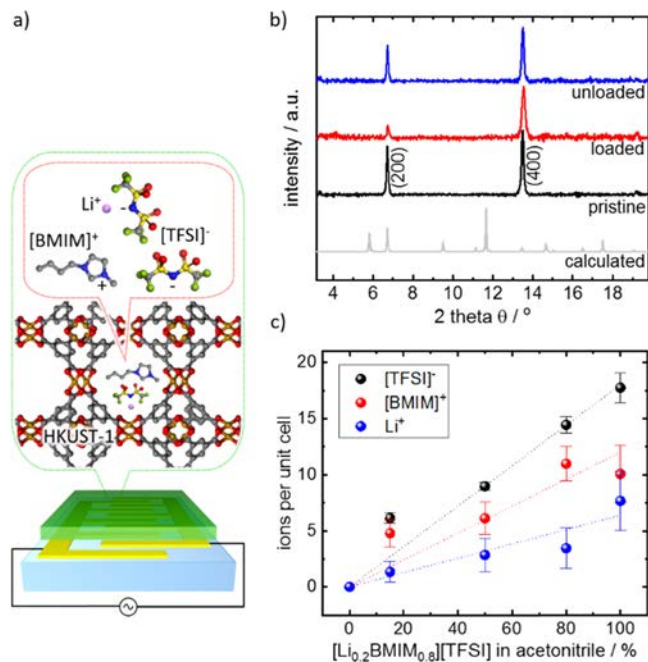


**Figure 1.** (a) Sketch of  $[Li_{0.2}BMIM_{0.8}][TFSI]$  IL in the pores of the HKUST 1 MOF thin films. For measuring the conductivity of IL@MOF via EIS, the MOF films were grown on glass substrates with deposited interdigitated gold electrodes. The color code for the atoms is as follows: C gray, O red, Cu orange, N blue, F green, S yellow, and Li violet. H is not shown. (b) X ray diffractograms of the pristine HKUST 1 SURMOF (black), the sample loaded with  $[Li_{0.2}BMIM_{0.8}][TFSI]$  (red) and after unloading the sample by rinsing with ethanol (blue) compared with the calculated data for the corresponding powder structure (gray). The experimentally observed diffraction peaks are labelled. (c) Concentration of  $[BMIM]^+$ ,  $[TFSI]^-$ , and  $Li^+$  in the SURMOF loaded from different  $[Li_{0.2}BMIM_{0.8}][TFSI]$ -acetonitrile solutions determined by energy dispersive X ray spectroscopy (EDX). The amounts of  $[TFSI]^-$  and  $[BMIM]^+$  relative to HKUST 1 are determined via fluorine, nitrogen, and copper. Based on the charge neutrality, the lithium amount is determined by the difference of  $[TFSI]^-$  and  $[BMIM]^+$ .

the IL@MOF pellets, we followed standard directions.<sup>47</sup> In detail, for each pellet, 220–430 mg of the material was placed inside a stainless steel press, and the pellet was formed under a pressure of approximately 150 MPa. The resulting pellets had cylindrical shapes of 13 mm diameter with a thickness of approximately 1.2–2.0 mm.

The X ray diffractograms were measured in an out of plane geometry using a Bruker D8 Advance diffractometer equipped with a position sensitive detector in the  $\theta$ - $2\theta$  geometry. A Cu anode with a wavelength of  $\lambda = 0.154$  nm was used.

Scanning electron microscopy (SEM) images were recorded with a TESCAN VEGA3 thermionic emission SEM system. The parameters are shown in the images in Figure S1. EDX with 8 kV accelerating voltage and 14 nm working distance was used to quantify the elements Cu, N, and F. For the EDX measurements, thick samples of approximately 1  $\mu$ m thickness were used.

**Measurement of Ionic Conduction Properties.** The electrochemical impedance spectra were measured with a Zurich Instruments MFIA impedance analyzer for a frequency range of 5 MHz–0.5 Hz. The SURMOF samples were placed in a homemade Teflon cell

where the interdigitated gold electrodes were contacted in a two probe way. The electric field between two (interdigitated) electrodes is approximately  $0.03$  V  $\mu$ m<sup>-1</sup>. The cell was purged with pure nitrogen with a flow rate of roughly 100 mL min<sup>-1</sup>. The impedance data, as shown in Figure 2, were recorded for two HKUST 1 SURMOF

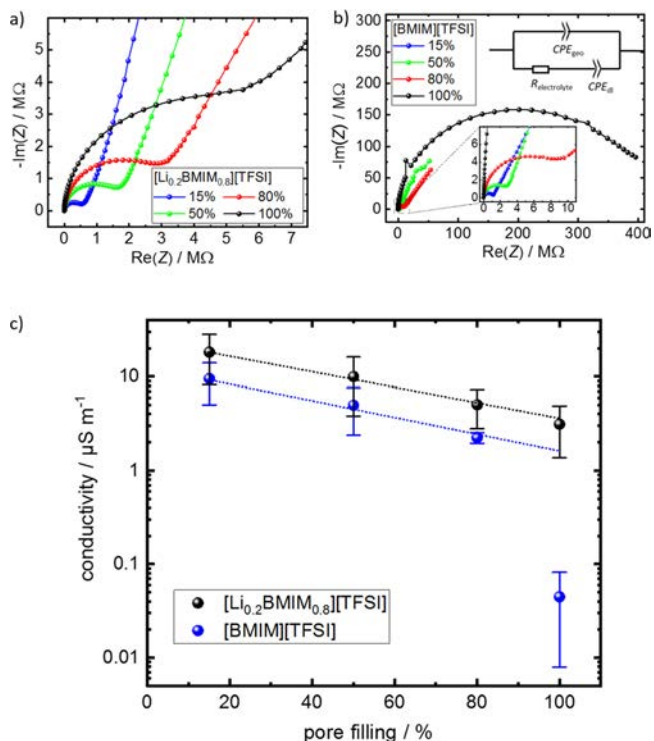


**Figure 2.** Nyquist plots of the impedance of the HKUST 1 SURMOF with various fillings of  $[Li_{0.2}BMIM_{0.8}][TFSI]$  (a) and  $[BMIM][TFSI]$  (b). The pore fillings are given in the legends. The frequency range is from 0.5 Hz to 5 MHz. All impedance spectra can be described with the reference circuit, composed of a constant phase element (CPE), representing the double layer capacitance at the electrode interface in series with an ohmic resistance, representing the resistance of the electrolyte in the nanoporous material, in parallel combination with a CPE, representing the geometric capacitance, as shown in the inset of panel (b). (c) Average values of the conductivities with the standard deviations as error bars. The black spheres are the conductivity of  $[Li_{0.2}BMIM_{0.8}][TFSI]$  and the blue spheres are that of  $[BMIM][TFSI]$ . The dotted lines represent the trend lines extrapolated for 15–80% loading. The ohmic resistance values are shown in Figure S2c.

samples. The IL concentration was varied in three consecutive cycles, first empty, then 15%, 50%, 80%, and finally 100% IL pore filling; first  $[BMIM][TFSI]$ , then  $[Li_{0.2}BMIM_{0.8}][TFSI]$ . The average values with the standard deviation as error bars are shown. All experiments were performed at room temperature (298 K).

The conduction of the pellets was measured by positioning the IL@MOF pellets between two planar electrodes, which are gold thin films (150 nm thickness) on conducting Si wafer. Using EIS in a frequency range from 5 MHz to 100 Hz, the ionic conductivities and the Ohmic resistances were determined from the Nyquist plots.

**MD Simulations.** The all atom MD simulations were carried out using the UFF4MOF force field, a MOF specific extension of Universal Force Field (UFF);<sup>48,49</sup> whereas for  $[BMIM][TFSI]$ , the well established all atom optimized potentials for liquid simulations (OPLS AA) compatible force field has been adopted from a previous study;<sup>50</sup> the parameterization of Li ions was adopted from OPLS AA. All simulations were performed utilizing the LAMMPS simulation package. The timestep of the simulation was set to  $\tau = 0.25$  fs, and the Nose–Hoover thermostat and Nose–Hoover–Andersen barostat

were used to model NPT conditions at ambient pressure ( $p = 1$  atm) and temperature ( $T = 300$  K). The packing calculation of the IL in the MOF was based on van der Waals sizes,<sup>51</sup> which is similar to the method used in our previous work.<sup>44</sup> This maximum packing can also be estimated based on the accessible pore volume of HKUST 1 (66%<sup>52</sup>) and an estimated average size of 276 cubic angstroms per ion pair for  $[\text{Li}_{0.2}\text{BMIM}_{0.8}][\text{TFSI}]$ , yielding approximately 21 pairs per unit cell, which is in good agreement with the maximum loading empirically achieved using the packing software package. The initial configuration of the simulation consists of a  $3 \times 3 \times 3$  supercell of the HKUST 1 unit cell, where ions are embedded within the MOF via a PACKmol software.<sup>50</sup> For the simulation protocol, we first performed energy minimization using the conjugate gradient method and run a 1 ns relaxation simulation without external electric field. For the production run, the mobility was computed in an external electric field in the (100) direction. Simulations with various loading factors ran for 5 ns each, where ions travel in the periodic simulation box driven by the external field. Because of the limited timescales of MD simulations, we have utilized a stronger electric field than that of the experiment setups.<sup>53,54</sup> To assess the effect of the stronger field, simulations were performed at various strengths of  $E = 8, 8.5, 10,$  and  $12.5 \text{ V nm}^{-1}$ . Because all investigated electric fields yield similar results, as shown in Figure S5, we focus on the field of  $8 \text{ V nm}^{-1}$  in the main part of the manuscript. The mobility of the IL was determined by measuring the  $\text{Li}^+$ ,  $[\text{BMIM}]^+$ , and  $[\text{TFSI}]^-$  drift velocity, and their respective contributions to the overall conductivity were calculated. The molar conductivity is kinetically derived as  $\Lambda_m = E^{-1}F\sum_i(q_i v_i)$ , where the  $i$ th component corresponds to  $\text{Li}^+$ ,  $[\text{BMIM}]^+$ , and  $[\text{TFSI}]^-$ .  $q$  is the charge of the ion,  $v$  is the drift velocity, and  $F$  is the Faraday constant.

## RESULTS AND DISCUSSION

**Experimental Data of Ionic Conduction.** The HKUST 1 SURMOF samples were prepared on glass substrates with interdigitated gold electrodes on the top using a LbL method, Figure 1a. The X ray diffraction (XRD) data (Figure 1b) show that the HKUST 1 SURMOF is grown in the (100) orientation on the substrate. The structure of the HKUST 1 SURMOF films was previously characterized in detail.<sup>33,39,55,56</sup> The nitrogen Brunauer–Emmett–Teller (BET) isotherm of such a HKUST 1 SURMOF film was explored for thin films grown on magnetic nanoparticles, which is in agreement with the BET isotherms of corresponding powders.<sup>57</sup> Upon IL loading, the XRD form factor changes, which is seen by the change of the (200):(400) intensity ratio. This is a clear indication for the loading of the IL in the MOF pores. Upon rinsing the IL loaded sample with ethanol for 20 min, a diffractogram similar to the diffractogram of the pristine sample is obtained, indicating IL release. The SEM image Figure S1 shows that the SURMOF film homogeneously covers the substrate. The film thickness is approximately  $0.4 \mu\text{m}$ .

The HKUST 1 SURMOF films were loaded with  $[\text{Li}_{0.2}\text{BMIM}_{0.8}][\text{TFSI}]$  IL from the IL–acetonitrile solutions of various concentrations. Acetonitrile was chosen as the solvent because of its mixability with the IL and its large vapor pressure at room temperature, resulting in a very high volatility. This means that it evaporates fast from the MOF pores, leaving IL solely in the pores. The fast acetonitrile evaporation from the MOF pores at room temperature in a nitrogen atmosphere was verified in a previous study.<sup>44</sup> Moreover, it has a very small conductivity, so the recorded conductivity can be exclusively attributed to the IL. For the  $[\text{BMIM}][\text{TFSI}]@\text{HKUST 1}$  reference system, the  $[\text{BMIM}][\text{TFSI}]$  IL is loaded in the same way in the same SURMOF sample.

The amounts of the  $[\text{Li}_{0.2}\text{BMIM}_{0.8}][\text{TFSI}]$  IL uptake by the SURMOF were quantified by EDX spectroscopy, Figure 1c. A maximum IL loading in the MOF of approximately  $18 \pm 1.5$   $[\text{Li}_{0.2}\text{BMIM}_{0.8}][\text{TFSI}]$  IL pairs per HKUST 1 MOF unit cell was estimated. The IL loading in the MOF pores is roughly proportional to the IL concentration in the solution. Based on this, we use the percentage of the IL in the acetonitrile solution to refer to the pore filling.

The conduction behavior of the IL@MOF was measured by EIS. The empty HKUST 1 sample, Figure S2a, essentially shows only a capacitive component of impedance, and an ohmic resistance in the order of  $10^{14} \Omega$  is estimated. Using the film thickness of approximately  $0.4 \mu\text{m}$ , a conductivity of roughly  $10^{-13} \text{ S m}^{-1}$  is approximated for the empty HKUST 1 MOF, which is in line with the values reported in the literature.<sup>58</sup>

The Nyquist plots of the same SURMOF sample with different IL pore fillings are shown in Figure 2a for  $[\text{Li}_{0.2}\text{BMIM}_{0.8}][\text{TFSI}]$  and in Figure 2b for the Li free  $[\text{BMIM}][\text{TFSI}]$  reference IL. In comparison to the empty SURMOF, the conductivities of all the IL loaded samples are many orders of magnitude larger, so the determined conductivity can be exclusively attributed to the IL ions. The EIS data are analyzed using the reference circuit shown in Figure 2b. The resulting conductivities are shown in Figure 2c. The conductivity of  $[\text{Li}_{0.2}\text{BMIM}_{0.8}][\text{TFSI}]$  shows a slight dependence of the pore filling. In detail, for 15 and 100% pore fillings, the conductivities are  $18.2 \pm 9.9$  and  $3.1 \pm 1.7 \mu\text{S m}^{-1}$ , respectively. In contrast, in the reference system, the conductivity of Li free  $[\text{BMIM}][\text{TFSI}]$  confined in HKUST 1 shows a drop of more than two orders of magnitude when filling the pores with IL. This tremendous drop of conductivity is caused by a mutual pore blockage of the relatively large cations and anions, which drift along the E field in opposite directions trying to simultaneously pass the pore windows.<sup>44</sup> This results in pore blocking, causing IL bunching and IL immobilization. More details of the ion bunching and pore blocking mechanism are given in our previous study.<sup>44</sup> It is worth noting that the conductivity of  $[\text{Li}_{0.2}\text{BMIM}_{0.8}][\text{TFSI}]$  is larger than that of  $[\text{BMIM}][\text{TFSI}]$  over the entire concentration range, being an indication that Li in  $[\text{Li}_{0.2}\text{BMIM}_{0.8}][\text{TFSI}]$  has a large mobility. At maximum loading, the conductivity of  $[\text{Li}_{0.2}\text{BMIM}_{0.8}][\text{TFSI}]$  in HKUST 1 is 70 times larger than that of  $[\text{BMIM}][\text{TFSI}]$ . This means that the presence of Li prevents the collapse of the conductivity at high loadings, as observed for the pure IL.

For comparison, the sample loaded with LiTFSI without  $[\text{BMIM}][\text{TFSI}]$  shows a conductivity of about  $47 \pm 5 \text{ nS m}^{-1}$ , which is two orders of magnitude lower than the conductivity of the  $[\text{Li}_{0.2}\text{BMIM}_{0.8}][\text{TFSI}]$  loaded SURMOF, Figure S2b. This indicates that the high Li conductivity in  $[\text{Li}_{0.2}\text{BMIM}_{0.8}][\text{TFSI}]$  is also based on the  $[\text{BMIM}]$  and  $[\text{TFSI}]$  ions, supposedly via a Grotthuss mechanism based on the  $[\text{TFSI}]$  anions.

For reference, we measured the conductivity of  $[\text{Li}_{0.2}\text{BMIM}_{0.8}][\text{TFSI}]$  in HKUST 1 powder pressed in the form of pellets, following the standard protocols, Figure S3.<sup>32,59–61</sup> The measured conductivity for the pellet samples increases by a factor of 50 when increasing the IL amount from 15 to 100%, Figure S4. These percentages are the ratio of the maximum pore fillings and correspond to the pore fillings shown in Figure 2. In addition to the opposite concentration dependence (compare Figure 2c and Figure S4), the total

values of the determined conductivities are more than one order of magnitude higher for the MOF powder pellets compared to the thin films.

**Simulation of Ionic Conduction.** For a detailed understanding of the ion mobility in the pores, the all atom MD simulations of  $[\text{Li}_{0.2}\text{BMIM}_{0.8}][\text{TFSI}]$  conductivity embedded in HKUST 1 were employed. For the specific loading of  $[\text{Li}_{0.2}\text{BMIM}_{0.8}][\text{TFSI}]$ , a maximum uptake at 21 IL pairs per MOF unit cell was determined using the packing algorithm described in the Methods section. The electrical external field is aligned in the (100) direction of HKUST 1, coinciding with the major axis of transport within the MOF. The conductivity for different pore fillings is shown in Figure 3. We find that the

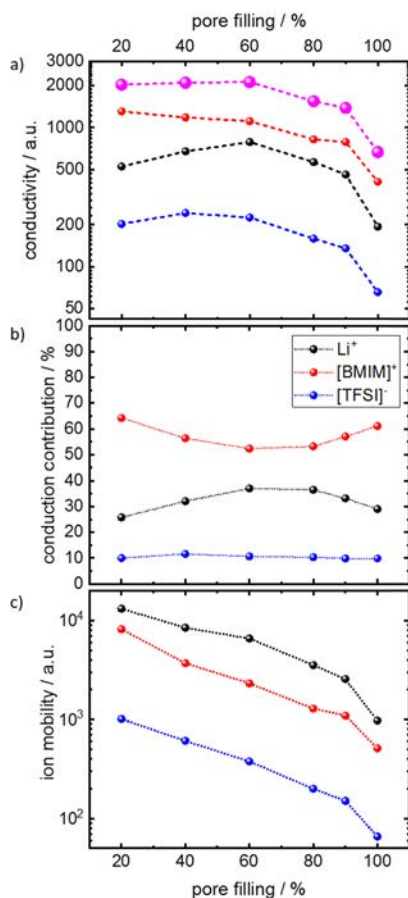


**Figure 3.** (a) Conductivity of  $[\text{Li}_{0.2}\text{BMIM}_{0.8}][\text{TFSI}]$  in HKUST 1 determined by MD simulations. The total conductivity is shown in magenta. The ion conductivities of  $[\text{BMIM}]^+$  in red,  $[\text{TFSI}]^-$  in blue, and  $\text{Li}^+$  in black. (b) Contribution of respective ions to the total conductivity. (c) Ion mobilities. The color codes in all the panels are identical.

conductivity of  $[\text{Li}_{0.2}\text{BMIM}_{0.8}][\text{TFSI}]$  decreases slightly, this means by about one third when increasing the pore filling from 20 to 90%. For fillings beyond 90%, there is an additional drop in conductivity by a factor of two. The MD simulations reproduce the concentration dependence of the conductivity measured with the thin film (SURMOF) model system, which is in contrast to the results from the MOF pellets, Figure S4.

The  $\text{Li}^+$  mobility is larger than the mobility of  $[\text{BMIM}]^+$  or  $[\text{TFSI}]^-$ .  $\text{Li}^+$  contributes approximately 26% to the overall conductivity at low loadings, whereas at medium loading (at 60 and 80%),  $\sim 37\%$  of the overall conductivity comes from  $\text{Li}^+$ ,

before being slightly reduced to 29% at full loading, as shown in Figure 3b. This is remarkable because only 10% of all ions are  $\text{Li}^+$ . In contrast to the decline in the conductivity of  $[\text{BMIM}]^+$  and  $[\text{TFSI}]^-$ , the conductivity of  $\text{Li}^+$  slightly increases with the filling degree, up to a pore filling value of 60–80%. This increases the contribution of  $\text{Li}^+$  to the overall conduction. Over the entire loading range, the contribution of  $[\text{BMIM}]^+$  to the entire conduction is larger than the contribution of  $\text{Li}^+$ , which is caused by the 4 times higher concentration of  $[\text{BMIM}]^+$  and its mobility, which is roughly half as large as the mobility of  $\text{Li}^+$ . The conduction of  $[\text{TFSI}]^-$  is much smaller than that of  $[\text{BMIM}]^+$  because of its molecular rigidity and size, and the contribution to the entire conductivity is small despite the fact that its number corresponds to the sum of  $\text{Li}^+$  and  $[\text{BMIM}]^+$ .

**Conduction Mechanism.** The statistical distribution of the distance between  $\text{Li}^+$  and  $[\text{TFSI}]^-$  exhibit a strong peak at 0.25 nm, Figure 4. This indicates a highly localized density of

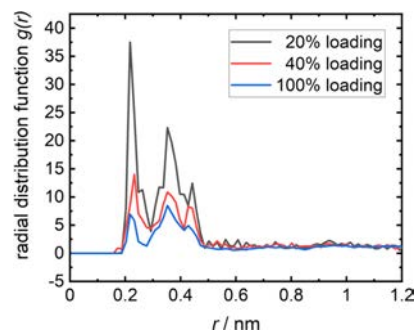


**Figure 4.** Radial distribution function of the distance between  $\text{Li}^+$  and  $[\text{TFSI}]^-$ . The maximum of the distribution is observed at about 0.25 nm.

$\text{Li}$  cations close to the  $[\text{TFSI}]^-$  anions, forming  $\text{Li}-\text{TFSI}$  complexes typical for a Grotthuss like conduction mechanism. The degree of  $\text{Li}$  ion localization decreases with increasing IL concentration because of a greater homogeneity of the charged IL environment. The Grotthuss like  $\text{Li}$  conduction is also visible in the videos of ion conduction, which are available online and presented in the Supporting Information S6. There, most  $\text{Li}$  cations are always in close proximity to the  $[\text{TFSI}]^-$  anions. The MD trajectories show that  $[\text{TFSI}]^-$  traps  $\text{Li}^+$  in their close proximity before  $\text{Li}^+$  is released, which is subsequently captured by the next anion. The Grotthuss like diffusion of  $\text{Li}$  ions in the solution was also found for other electrolytes.<sup>62–64</sup>

In contrast to the Grotthuss like conduction of  $\text{Li}$  cations,  $[\text{TFSI}]^-$  anions and  $[\text{BMIM}]^+$  cations show an individual vehicular mechanism. This is presumably caused by the larger molecular size and the charge delocalization over the molecule, resulting in smaller local electric fields.

A closer inspection of the MD simulation data reveals further details of the conduction mechanism. All ions are singly charged, and their motions are driven by the external field with equal force, although in opposite directions. For  $[\text{BMIM}]^+$  and  $[\text{TFSI}]^-$ , because of their relatively large molecular size and narrow MOF pore windows, their mobility decreased with increasing loading. For highest loadings,  $[\text{BMIM}]^+$  and  $[\text{TFSI}]^-$  form a bunched layer whose ion density becomes so high that the transport is strongly decelerated. These findings are qualitatively similar to prior work, where we found

bunching and pore jamming of [BMIM][TFSI] IL at high loading, leading to a drastic drop in the overall conductivity.<sup>44</sup> Compared to pure [BMIM][TFSI], the bunched ion layer is also present while the mobility drop of [BMIM]<sup>+</sup> and [TFSI]<sup>-</sup> in [Li<sub>0.2</sub>BMIM<sub>0.8</sub>][TFSI] in HKUST 1 is reduced. At an external field of  $E = 8 \text{ V nm}^{-1}$ , the conductivity drop subjected to bunching is 1.9× for [BMIM]<sup>+</sup>, 2.1× for [TFSI]<sup>-</sup>, and 2.4× for Li<sup>+</sup>, while the combined effect is a conductivity drop by a factor of 2.07, comparing the conductivities at 90 and 100% pore filling. At high loadings, while in the bunched layer, the Lennard Jones interaction contributes to more than 85% of the interaction potential for the organic IL molecules, and this value is less than 2% for Li<sup>+</sup>. Noteworthy, the interaction between the ion guests and the MOF, in particular, the metal node, was found to have only minor contributions. In detail, the electrostatic IL MOF interaction contributes to 14.9% of the overall interaction potential in the bunched layer. For Li<sup>+</sup>, the interaction with [TFSI]<sup>-</sup> is more than 3 times stronger than that with the MOF.

The snapshots of the ion conduction of [Li<sub>0.2</sub>BMIM<sub>0.8</sub>][TFSI] in HKUST 1 at low and high loadings are shown in Figure 5a,b. The corresponding analysis of the ion distribution is shown in Figure 5c,d. At low loadings, the ion distribution and transport are homogeneous for [BMIM]<sup>+</sup>, [TFSI]<sup>-</sup>, and Li<sup>+</sup>. At high loadings, the formation of a bunched ion layer results in an inhomogeneous distribution of all types of ions: [BMIM]<sup>+</sup> resides on the side closer to the anode, aiming to move toward the cathode. [TFSI]<sup>-</sup> accumulates closer to the cathode, aiming to move toward the anode. The Li cations show an affinity to the [TFSI]<sup>-</sup>, and the drift is accomplished in short range hopping events between the [TFSI] anions.

The comparison of the ion concentration with the Li free IL reference system at low and maximum loadings (Figure 5e,f) shows that the concentration inhomogeneity and ion bunching of [Li<sub>0.2</sub>BMIM<sub>0.8</sub>][TFSI] in HKUST 1 are less pronounced than those of [BMIM][TFSI] in HKUST 1. In detail, while the ratio of the maximum to minimum ion concentration is 63 for [TFSI]<sup>-</sup> and 79 for [BMIM]<sup>+</sup> in [BMIM][TFSI] in HKUST 1 at full loading (mainly caused by the small density in between the high density zones), these ratios are only 18 and 12, respectively, for fully loaded [Li<sub>0.2</sub>BMIM<sub>0.8</sub>][TFSI] in HKUST 1. It is worth noting that the Li distribution is relatively homogeneous, fluctuating between 2.0 and 6.7 ions per unit cell, giving a maximum to minimum ion concentration ratio of 3.4. While the minimum Li<sup>+</sup> concentration is located at the highest [BMIM]<sup>+</sup> concentration, the highest Li<sup>+</sup> concentration is located in the zones with low [BMIM]<sup>+</sup> and high [TFSI]<sup>-</sup> concentrations. This means that the accumulation of [BMIM] cations is found to prevent Li<sup>+</sup> passage via electrostatic repulsion, while the anions accumulate on the other side of the bunched region, capturing Li<sup>+</sup>. As a result, the Li<sup>+</sup> conduction decreases between 80 and 100% pore filling, see Figure 3b.

In comparison to [BMIM][TFSI], the lower strength of ion bunching in [Li<sub>0.2</sub>BMIM<sub>0.8</sub>][TFSI] is caused by Li<sup>+</sup> forming charge neutral Li TFSI complexes, which is not being accelerated by the electric field and not contributing to ion bunching. Thus, the small amount of Li<sup>+</sup> (only 10% of the ions) is the reason why the tremendous drop of conductivity at maximum pore loading is not observed.

The trajectories of the ions in the MOF are shown in Figure 6. The long residence time of Li<sup>+</sup> when bound to anions can be seen by the steplike plateaus in individual ion trajectories. The

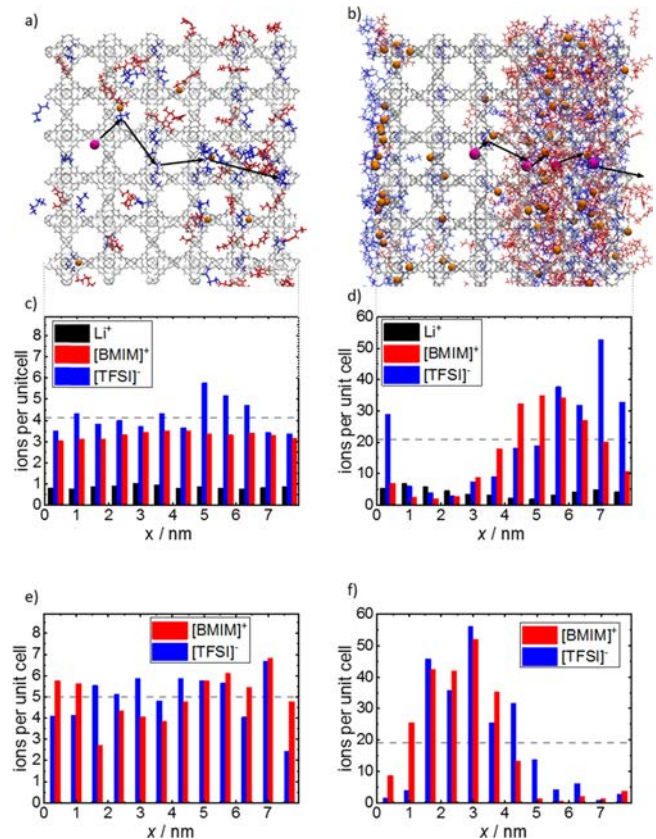


**Figure 5.** Snapshot of the ions of [Li<sub>0.2</sub>BMIM<sub>0.8</sub>][TFSI] in HKUST 1 at 20% (a) and 100% (b) loading. The ions are labeled in different colors: [BMIM]<sup>+</sup> red, [TFSI]<sup>-</sup> blue, and Li<sup>+</sup> as orange. The external electric field is horizontal, pointing to the left. 3×3×3 unit cells are shown. Tracer Li ions are marked in violet, and the steps in the following 2.5 ps are indicated by arrows. At the Grotthuss like hopping illustrated in (b), a chain of four Li ions travel left to right, before being localized near the [TFSI] anions, in turn dislocating the next Li<sup>+</sup>. (c) and (d) Ion densities averaged over 2.5 ps time interval. The average ion densities are indicated by the dashed line. The ion distribution of the Li free reference system (that is, [BMIM][TFSI] in HKUST 1) under identical conditions is shown in panel (e) and (f).

localization is followed by a release and free movement of Li<sup>+</sup> to the next anion, which contrasts vividly with the diffusion of the [BMIM] cations in the trajectories. For low loadings, the pronounced formation of cation–anion pairs between Li<sup>+</sup> and [TFSI]<sup>-</sup> reduces the conductivity of Li<sup>+</sup>. With increasing IL loadings, the plateaus in Li<sup>+</sup> transport are greatly reduced, whereas [BMIM]<sup>+</sup> and [TFSI]<sup>-</sup> exhibit transient jamming. At high loadings, [BMIM]<sup>+</sup> and [TFSI]<sup>-</sup> exhibit long plateaus, indicating very long residence times within bunched layers caused by the blocked pores.<sup>44</sup> Although the mechanism for the stop and go like transport differs, the trajectories of Li<sup>+</sup> at low loadings are similar to the trajectories of [BMIM]<sup>+</sup> and [TFSI]<sup>-</sup> at high loadings.

The MD simulations of Li IL with varying Li contents are shown in Figure S7. The data show that the Li<sup>+</sup> mobility increases with the increasing Li content for MOFs with maximum Li IL loading. In the corresponding experiment, the loading of the SURMOF with maximum pore fillings of LiTFSI (by saturated LiTFSI solutions) destabilizes the MOF thin film. Thus, no solid experimental reference data are available, and the in depth exploration of the conduction at different Li

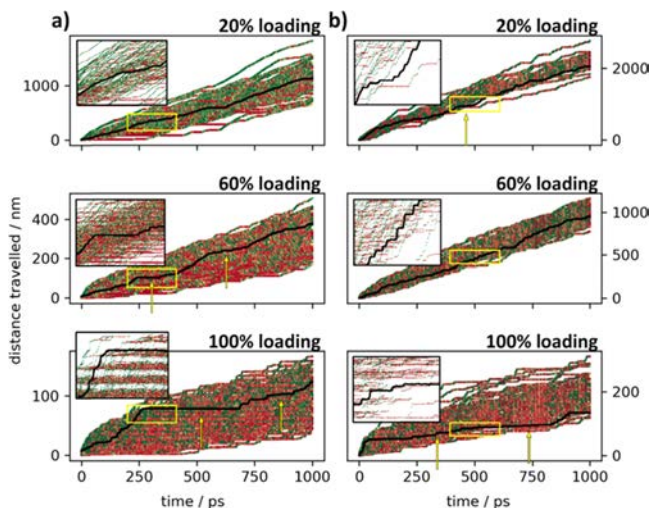


**Figure 6.** Trajectories of individual  $[\text{BMIM}]^+$  (a) and  $\text{Li}^+$  (b) ions at low, medium, and high loadings. Typical tracer trajectories are marked in black, whereas for the rest of the ions and the trajectories are color coded with respect to their temporal drift speed. Green corresponds to a drift faster than the average mobility of  $[\text{BMIM}]^+$ ,  $\text{Li}^+$ , and  $[\text{TFSI}]^+$  at the corresponding loading. Red corresponds to a slower drift. Arrows indicate plateaus in the tracer trajectories which correspond to long local residence. For the rest of the ions, the switching patterns of green–red–green correspond to such intermittent hopping. The insets show zoomed images of a 200 ps time window (yellow boxes).

TFSI ratios in an appropriate model system remains to be a task for future studies.

## CONCLUSIONS

In order to characterize the conductivity of MOFs loaded with ILs as separators for LIBs and as solid state electrolytes, we investigated the conduction of a Li based IL in the nanopores of crystalline MOFs experimentally and by MD simulations. We find strikingly different behaviors for samples using MOF powder pressed into pellets and MOF films. In the former, the conductance increases dramatically with loading, but this is attributed to excess IL in the pellets. In contrast, the conductance in MOF films can be purely attributed to the IL in the pores and shows a complex behavior. The conductivity of  $[\text{Li}_{0.2}\text{BMIM}_{0.8}][\text{TFSI}]$  in HKUST 1 only slightly decreases by less than one order of magnitude, with increasing pore loading. This is in contrast to the conduction of the Li free reference ionic liquid, that is, pure  $[\text{BMIM}][\text{TFSI}]$ , whose conductivity drops by more than two orders of magnitude with increasing pore filling, and the ions show pore blocking and ion bunching behavior. MD simulations show a Grotthuss like charge transfer of  $\text{Li}^+$  with a high mobility, contributing to about 26 to 37% of the total conductivity. At high loadings,  $[\text{BMIM}]^+$  and  $[\text{TFSI}]^-$  also show a bunching behavior for  $[\text{Li}_{0.2}\text{BMIM}_{0.8}][\text{TFSI}]@$ HKUST 1, immobilizing these ions and also decreasing the  $\text{Li}^+$  conductivity. Because of the formation of neutral Li–TFSI complexes, the ion bunching and pore blocking behaviors are significantly attenuated. As a result, the total conductivity only slightly decreases with pore loading, and at full loadings, the conduction of the Li containing IL is about two orders of magnitude larger in comparison to the Li free reference IL.

The unveiled details of charge transfer contribute to a better understanding of the conduction in solid state electrolytes

composed of nanoporous materials with embedded ionic liquids. For instance, by adjusting the Li IL ratio, the exploitation of microscopic details may contribute to an improved performance of nanoporous materials as separators in Li based batteries.

## AUTHOR INFORMATION

### Corresponding Authors

**Wolfgang Wenzel** – Karlsruhe Institute of Technology (KIT),  
Institute of Nanotechnology (INT), Eggenstein Leopoldshafen  
76344, Germany; Email: Wolfgang.Wenzel@kit.edu

**Lars Heinke** – Karlsruhe Institute of Technology (KIT),  
Institute of Functional Interfaces (IFG), Eggenstein  
Leopoldshafen 76344, Germany; Email: Lars.Heinke@  
kit.edu

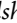
### Authors

**Micaela Vazquez** – Karlsruhe Institute of Technology (KIT),  
Institute of Functional Interfaces (IFG), Eggenstein  
Leopoldshafen 76344, Germany

**Modan Liu** – Karlsruhe Institute of Technology (KIT),  
Institute of Nanotechnology (INT), Eggenstein Leopoldshafen  
76344, Germany

**Zejun Zhang** – Karlsruhe Institute of Technology (KIT),  
Institute of Functional Interfaces (IFG), Eggenstein  
Leopoldshafen 76344, Germany

**Abhinav Chandresh** – Karlsruhe Institute of Technology  
(KIT), Institute of Functional Interfaces (IFG), Eggenstein  
Leopoldshafen 76344, Germany

**Anemar Bruno Kanj** – Karlsruhe Institute of Technology  
(KIT), Institute of Functional Interfaces (IFG), Eggenstein  
Leopoldshafen 76344, Germany;  orcid.org/0000 0001  
6385 4634

### Author Contributions

<sup>‡</sup>M.V. and M.L. contributed equally.

### Author Contributions

The manuscript was written through contributions of all authors. All authors have given approval to the final version of the manuscript.

### Notes

The authors declare no competing financial interest.

## ACKNOWLEDGMENTS

The authors gratefully acknowledge funding by the Volkswagen Foundation, the Fonds der Chemischen Industrie, and the German Science Foundation (DFG HE 7036/5, SPP 1928 COORNETs, SFB 1176, and EXC2082).

## REFERENCES

- (1) Francis, C. F. J.; Kyratzis, I. L.; Best, A. S. Lithium Ion Battery Separators for Ionic Liquid Electrolytes: A Review. *Adv. Mater.* **2020**, *32*, No. 1904205.
- (2) Abada, S.; Marlair, G.; Lecocq, A.; Petit, M.; Sauvant Moynot, V.; Huet, F. Safety Focused Modeling of Lithium Ion Batteries: A Review. *J. Power Sources* **2016**, *306*, 178–192.
- (3) Hallett, J. P.; Welton, T. Room Temperature Ionic Liquids: Solvents for Synthesis and Catalysis. 2. *Chem. Rev.* **2011**, *111*, 3508–3576.
- (4) MacFarlane, D. R.; Tachikawa, N.; Forsyth, M.; Pringle, J. M.; Howlett, P. C.; Elliott, G. D.; Davis, J. H.; Watanabe, M.; Simon, P.; Angell, C. A. Energy Applications of Ionic Liquids. *Energy Environ. Sci.* **2014**, *7*, 232–250.
- (5) Smiglak, M.; Pringle, J. M.; Lu, X.; Han, L.; Zhang, S.; Gao, H.; MacFarlane, D. R.; Rogers, R. D. Ionic Liquids for Energy, Materials, and Medicine. *Chem. Commun.* **2014**, *50*, 9228–9250.
- (6) Passos, H.; Freire, M. G.; Coutinho, J. A. P. Ionic Liquid Solutions as Extractive Solvents for Value Added Compounds from Biomass. *Green Chem.* **2014**, *16*, 4786–4815.
- (7) Elia, G. A.; Ulissi, U.; Jeong, S.; Passerini, S.; Hassoun, J. Exceptional Long Life Performance of Lithium Ion Batteries Using Ionic Liquid Based Electrolytes. *Energy Environ. Sci.* **2016**, *9*, 3210–3220.
- (8) Balducci, A. Ionic Liquids in Lithium Ion Batteries. *Top. Curr. Chem.* **2017**, *375*, 20.
- (9) Chmiola, J.; Yushin, G.; Gogotsi, Y.; Portet, C.; Simon, P.; Taberna, P. L. Anomalous Increase in Carbon Capacitance at Pore Sizes Less Than 1 Nanometer. *Science* **2006**, *313*, 1760–1763.
- (10) Merlet, C.; Rotenberg, B.; Madden, P. A.; Taberna, P. L.; Simon, P.; Gogotsi, Y.; Salanne, M. On the Molecular Origin of Supercapacitance in Nanoporous Carbon Electrodes. *Nat. Mater.* **2012**, *11*, 306–310.
- (11) Futamura, R.; Iiyama, T.; Takasaki, Y.; Gogotsi, Y.; Biggs, M. J.; Salanne, M.; Ségalini, J.; Simon, P.; Kaneko, K. Partial Breaking of the Coulombic Ordering of Ionic Liquids Confined in Carbon Nanopores. *Nat. Mater.* **2017**, *16*, 1225.
- (12) Sheng, Z.; Zhang, J.; Liu, J.; Zhang, Y.; Chen, X.; Hou, X. Liquid Based Porous Membranes. *Chem. Soc. Rev.* **2020**, *49*, 7907–7928.
- (13) Sheng, Z.; Wang, H.; Tang, Y.; Wang, M.; Huang, L.; Min, L.; Meng, H.; Chen, S.; Jiang, L.; Hou, X. Liquid Gating Elastomeric Porous System with Dynamically Controllable Gas/Liquid Transport. *Sci. Adv.* **2018**, *4*, No. eaao6724.
- (14) Cheng, C.; Jiang, G.; Simon, G. P.; Liu, J. Z.; Li, D. Low Voltage Electrostatic Modulation of Ion Diffusion through Layered Graphene Based Nanoporous Membranes. *Nat. Nanotechnol.* **2018**, *13*, 685.
- (15) Park, S.; Moilanen, D. E.; Fayer, M. D. Water Dynamic Effects of Ions and Nanoconfinement. *J. Phys. Chem. B* **2008**, *112*, 5279–5290.
- (16) Nazari, M.; Davoodabadi, A.; Huang, D.; Luo, T.; Ghasemi, H. Transport Phenomena in Nano/Molecular Confinements. *ACS Nano* **2020**, *14*, 16348–16391.
- (17) Furukawa, H.; Cordova, K. E.; O’Keeffe, M.; Yaghi, O. M. The Chemistry and Applications of Metal Organic Frameworks. *Science* **2013**, *341*, No. 1230444.
- (18) Kaskel, S., *The Chemistry of Metal Organic Frameworks: Synthesis, Characterization, and Applications*. Wiley: 2016; 904.
- (19) Bundschuh, S.; Kraft, O.; Arslan, H. K.; Gliemann, H.; Weidler, P. G.; Wöll, C. Mechanical Properties of Metal Organic Frameworks: An Indentation Study on Epitaxial Thin Films. *Appl. Phys. Lett.* **2012**, *101*, 101910.
- (20) Haldar, R.; Heinke, L.; Wöll, C. Advanced Photoresponsive Materials Using the Metal–Organic Framework Approach. *Adv. Mater.* **2020**, *32*, No. 1905227.
- (21) Neumann, T.; Liu, J.; Wächter, T.; Friederich, P.; Symalla, F.; Welle, A.; Mugnaini, V.; Meded, V.; Zharnikov, M.; Wöll, C.; Wenzel, W. Superexchange Charge Transport in Loaded Metal Organic Frameworks. *ACS Nano* **2016**, *10*, 7085–7093.
- (22) Dhakshinamoorthy, A.; Li, Z.; Garcia, H. Catalysis and Photocatalysis by Metal Organic Frameworks. *Chem. Soc. Rev.* **2018**, *47*, 8134–8172.
- (23) Chen, N.; Li, Y.; Dai, Y.; Qu, W.; Xing, Y.; Ye, Y.; Wen, Z.; Guo, C.; Wu, F.; Chen, R. A Li+ Conductive Metal Organic Framework Electrolyte Boosts the High Temperature Performance of Dendrite Free Lithium Batteries. *J. Mater. Chem. A* **2019**, *7*, 9530–9536.
- (24) Angulakshmi, N.; Kumar, R. S.; Kulandainathan, M. A.; Stephan, A. M. Composite Polymer Electrolytes Encompassing Metal Organic Frameworks: A New Strategy for All Solid State Lithium Batteries. *J. Phys. Chem. C* **2014**, *118*, 24240–24247.
- (25) Gerbaldi, C.; Nair, J. R.; Kulandainathan, M. A.; Kumar, R. S.; Ferrara, C.; Mustarelli, P.; Stephan, A. M. Innovative High Performing Metal Organic Framework (Mof) Laden Nanocomposite Polymer Electrolytes for All Solid State Lithium Batteries. *J. Mater. Chem. A* **2014**, *2*, 9948–9954.
- (26) Angulakshmi, N.; Zhou, Y.; Suriyakumar, S.; Dhanalakshmi, R. B.; Satishrajan, M.; Alwarappan, S.; Alkordi, M. H.; Stephan, A. M. Microporous Metal Organic Framework (Mof) Based Composite Polymer Electrolyte (Cpe) Mitigating Lithium Dendrite Formation in All Solid State Lithium Batteries. *ACS Omega* **2020**, *5*, 7885–7894.
- (27) Fan, L.; Guo, Z.; Zhang, Y.; Wu, X.; Zhao, C.; Sun, X.; Yang, G.; Feng, Y.; Zhang, N. Stable Artificial Solid Electrolyte Interphase Films for Lithium Metal Anode Via Metal Organic Frameworks Cemented by Polyvinyl Alcohol. *J. Mater. Chem. A* **2020**, *8*, 251–258.
- (28) Han, D. D.; Wang, Z. Y.; Pan, G. L.; Gao, X. P. Metal Organic Framework Based Gel Polymer Electrolyte with Immobilized Anions to Stabilize a Lithium Anode for a Quasi Solid State Lithium Sulfur Battery. *ACS Appl. Mater. Interfaces* **2019**, *11*, 18427–18435.
- (29) Malik, R.; Loveridge, M. J.; Williams, L. J.; Huang, Q.; West, G.; Shearing, P. R.; Bhagat, R.; Walton, R. I. Porous Metal Organic Frameworks for Enhanced Performance Silicon Anodes in Lithium Ion Batteries. *Chem. Mater.* **2019**, *31*, 4156–4165.
- (30) Wang, Z.; Tan, R.; Wang, H.; Yang, L.; Hu, J.; Chen, H.; Pan, F. A Metal Organic Framework Based Electrolyte with Nanowetted Interfaces for High Energy Density Solid State Lithium Battery. *Adv. Mater.* **2018**, *30*, No. 1704436.
- (31) Yoshida, Y.; Fujie, K.; Lim, D. W.; Ikeda, R.; Kitagawa, H. Superionic Conduction over a Wide Temperature Range in a Metal Organic Framework Impregnated with Ionic Liquids. *Angew. Chem., Int. Ed.* **2019**, *58*, 10909–10913.
- (32) Fujie, K.; Ikeda, R.; Otsubo, K.; Yamada, T.; Kitagawa, H. Lithium Ion Diffusion in a Metal Organic Framework Mediated by an Ionic Liquid. *Chem. Mater.* **2015**, *27*, 7355–7361.
- (33) Shekha, O.; Wang, H.; Kowarik, S.; Schreiber, F.; Paulus, M.; Tolan, M.; Sternemann, C.; Evers, F.; Zacher, D.; Fischer, R. A.; Wöll, C. Step by Step Route for the Synthesis of Metal Organic Frameworks. *J. Am. Chem. Soc.* **2007**, *129*, 15118–15119.
- (34) Heinke, L.; Wöll, C. Surface Mounted Metal–Organic Frameworks: Crystalline and Porous Molecular Assemblies for Fundamental Insights and Advanced Applications. *Adv. Mater.* **2019**, *31*, No. 1806324.
- (35) Osada, I.; de Vries, H.; Scrosati, B.; Passerini, S. Ionic Liquid Based Polymer Electrolytes for Battery Applications. *Angew. Chem., Int. Ed.* **2016**, *55*, 500–513.
- (36) Tamilarasan, P.; Ramaprabhu, S. Graphene Based All Solid State Supercapacitors with Ionic Liquid Incorporated Polyacrylonitrile Electrolyte. *Energy* **2013**, *51*, 374–381.



- (37) Monti, D.; Jónsson, E.; Palacín, M. R.; Johansson, P. Ionic Liquid Based Electrolytes for Sodium Ion Batteries: Na<sup>+</sup> Solvation and Ionic Conductivity. *J. Power Sources* **2014**, *245*, 630–636.
- (38) Chui, S. S. Y.; Lo, S. M. F.; Charmant, J. P. H.; Orpen, A. G.; Williams, I. D. A Chemically Functionalizable Nanoporous Material Cu<sub>3</sub>(Tma)<sub>2</sub>(H<sub>2</sub>O)<sub>3</sub> (N). *Science* **1999**, *283*, 1148–1150.
- (39) Wang, Z.; Weidler, P. G.; Azucena, C.; Heinke, L.; Wöll, C. Negative, Anisotropic Thermal Expansion in Monolithic Thin Films of Crystalline Metal Organic Frameworks. *Microporous Mesoporous Mater.* **2016**, *222*, 241–246.
- (40) Shen, L.; Wu, H. B.; Liu, F.; Brosmer, J. L.; Shen, G.; Wang, X.; Zink, J. I.; Xiao, Q.; Cai, M.; Wang, G.; Lu, Y.; Dunn, B. Creating Lithium Ion Electrolytes with Biomimetic Ionic Channels in Metal–Organic Frameworks. *Adv. Mater.* **2018**, *30*, No. 1707476.
- (41) Bai, S.; Liu, X.; Zhu, K.; Wu, S.; Zhou, H. Metal Organic Framework Based Separator for Lithium Sulfur Batteries. *Nat. Energy* **2016**, *1*, No. 16094.
- (42) Baumann, A. E.; Aversa, G. E.; Roy, A.; Falk, M. L.; Bedford, N. M.; Thoi, V. S. Promoting Sulfur Adsorption Using Surface Cu Sites in Metal Organic Frameworks for Lithium Sulfur Batteries. *J. Mater. Chem. A* **2018**, *6*, 4811–4821.
- (43) Wang, Z.; Li, X.; Cui, Y.; Yang, Y.; Pan, H.; Wang, Z.; Wu, C.; Chen, B.; Qian, G. A Metal Organic Framework with Open Metal Sites for Enhanced Confinement of Sulfur and Lithium Sulfur Battery of Long Cycling Life. *Cryst. Growth Des.* **2013**, *13*, 5116–5120.
- (44) Kanj, A. B.; Verma, R.; Liu, M.; Helfferich, J.; Wenzel, W.; Heinke, L. Bunching and Immobilization of Ionic Liquids in Nanoporous Metal–Organic Framework. *Nano Lett.* **2019**, *19*, 2114–2120.
- (45) Gu, Z. G.; Pfriem, A.; Hamsch, S.; Breitwieser, H.; Wohlgemuth, J.; Heinke, L.; Gliemann, H.; Wöll, C. Transparent Films of Metal Organic Frameworks for Optical Applications. *Microporous Mesoporous Mater.* **2015**, *211*, 82–87.
- (46) Al Janabi, N.; Hill, P.; Torrente Murciano, L.; Garforth, A.; Gorgojo, P.; Siperstein, F.; Fan, X. Mapping the Cu Btc Metal Organic Framework (Hkust-1) Stability Envelope in the Presence of Water Vapour for CO<sub>2</sub> Adsorption from Flue Gases. *Chem. Eng. J.* **2015**, *281*, 669–677.
- (47) Panda, D. K.; Maity, K.; Palukoshka, A.; Ibrahim, F.; Saha, S. Li<sup>+</sup> Ion Conducting Sulfonate Based Neutral Metal Organic Framework. *ACS Sustainable Chem. Eng.* **2019**, *7*, 4619–4624.
- (48) Coupry, D. E.; Addicoat, M. A.; Heine, T. Extension of the Universal Force Field for Metal Organic Frameworks. *J. Chem. Theory Comput.* **2016**, *12*, 5215–5225.
- (49) Boyd, P. G.; Moosavi, S. M.; Witman, M.; Smit, B. Force Field Prediction of Materials Properties in Metal Organic Frameworks. *J. Phys. Chem. Lett.* **2017**, *8*, 357–363.
- (50) Li, Z.; Xiao, Y.; Xue, W.; Yang, Q.; Zhong, C. Ionic Liquid/Metal Organic Framework Composites for H<sub>2</sub>S Removal from Natural Gas: A Computational Exploration. *J. Phys. Chem. C* **2015**, *119*, 3674–3683.
- (51) Zhao, Y. H.; Abraham, M. H.; Zissimos, A. M. Fast Calculation of Van Der Waals Volume as a Sum of Atomic and Bond Contributions and Its Application to Drug Compounds. *J. Org. Chem.* **2003**, *68*, 7368–7373.
- (52) Rowsell, J. L. C.; Yaghi, O. M. Effects of Functionalization, Catenation, and Variation of the Metal Oxide and Organic Linking Units on the Low Pressure Hydrogen Adsorption Properties of Metal–Organic Frameworks. *J. Am. Chem. Soc.* **2006**, *128*, 1304–1315.
- (53) Miao, J.; Bhatta, R. S.; Reneker, D. H.; Tsige, M.; Taylor, P. L. Molecular Dynamics Simulations of Relaxation in Stretched PvdF Nanofibers. *Polymer* **2015**, *56*, 482–489.
- (54) Xu, W. J.; He, C. T.; Ji, C. M.; Chen, S. L.; Huang, R. K.; Lin, R. B.; Xue, W.; Luo, J. H.; Zhang, W. X.; Chen, X. M. Molecular Dynamics of Flexible Polar Cations in a Variable Confined Space: Toward Exceptional Two Step Nonlinear Optical Switches. *Adv. Mater.* **2016**, *28*, 5886–5890.
- (55) Shekhah, O.; Wang, H.; Strunskus, T.; Cyganik, P.; Zacher, D.; Fischer, R.; Wöll, C. Layer by Layer Growth of Oriented Metal Organic Polymers on a Functionalized Organic Surface. *Langmuir* **2007**, *23*, 7440–7442.
- (56) Müller, K.; Vankova, N.; Schöttner, L.; Heine, T.; Heinke, L. Dissolving Uptake Hindering Surface Defects in Metal Organic Frameworks. *Chem. Sci.* **2019**, *10*, 153–160.
- (57) Silvestre, M. E.; Franzreb, M.; Weidler, P. G.; Shekhah, O.; Wöll, C. Magnetic Cores with Porous Coatings: Growth of Metal Organic Frameworks on Particles Using Liquid Phase Epitaxy. *Adv. Funct. Mater.* **2013**, *23*, 1210–1213.
- (58) Liu, J.; Wächter, T.; Irmeler, A.; Weidler, P. G.; Gliemann, H.; Pauly, F.; Mugnaini, V.; Zharnikov, M.; Wöll, C. Electric Transport Properties of Surface Anchored Metal–Organic Frameworks and the Effect of Ferrocene Loading. *ACS Appl. Mater. Interfaces* **2015**, *7*, 9824–9830.
- (59) Xu, Q.; Zhang, X.; Zeng, S.; Bai, L.; Zhang, S. Ionic Liquid Incorporated Metal Organic Framework for High Ionic Conductivity over Extended Temperature Range. *ACS Sustainable Chem. Eng.* **2019**, *7*, 7892–7899.
- (60) Kinik, F. P.; Uzun, A.; Keskin, S. Ionic Liquid/Metal Organic Framework Composites: From Synthesis to Applications. *ChemSusChem* **2017**, *10*, 2842–2863.
- (61) Fujie, K.; Kitagawa, H. Ionic Liquid Transported into Metal Organic Frameworks. *Coord. Chem. Rev.* **2016**, *307*, 382–390.
- (62) Hwang, S.; Kim, D. H.; Shin, J. H.; Jang, J. E.; Ahn, K. H.; Lee, C.; Lee, H. Ionic Conduction and Solution Structure in Lipf<sub>6</sub> and Libf<sub>4</sub> Propylene Carbonate Electrolytes. *J. Phys. Chem. C* **2018**, *122*, 19438–19446.
- (63) Yim, C. H.; Tam, J.; Soboleski, H.; Abu Lebdeh, Y. On the Correlation between Free Volume, Phase Diagram and Ionic Conductivity of Aqueous and Non Aqueous Lithium Battery Electrolyte Solutions over a Wide Concentration Range. *J. Electrochem. Soc.* **2017**, *164*, A1002–A1011.
- (64) Dokko, K.; Watanabe, D.; Ugata, Y.; Thomas, M. L.; Tsuzuki, S.; Shinoda, W.; Hashimoto, K.; Ueno, K.; Umebayashi, Y.; Watanabe, M. Direct Evidence for Li Ion Hopping Conduction in Highly Concentrated Sulfolane Based Liquid Electrolytes. *J. Phys. Chem. B* **2018**, *122*, 10736–10745.

## Repository KITopen

Dies ist ein Postprint/begutachtetes Manuskript.

Empfohlene Zitierung:

Vazquez, M.; Liu, M.; Zhang, Z.; Chandresh, A.; Kanj, A. B.; Wenzel, W.; Heinke, L.  
[Structural and Dynamic Insights into the Conduction of Lithium-Ionic-Liquid Mixtures in Nanoporous Metal-Organic Frameworks as Solid-State Electrolytes](#)  
2021. ACS Applied Materials and Interfaces  
[doi:10.5445/IR/1000133857](https://doi.org/10.5445/IR/1000133857)

Zitierung der Originalveröffentlichung:

Vazquez, M.; Liu, M.; Zhang, Z.; Chandresh, A.; Kanj, A. B.; Wenzel, W.; Heinke, L.  
[Structural and Dynamic Insights into the Conduction of Lithium-Ionic-Liquid Mixtures in Nanoporous Metal-Organic Frameworks as Solid-State Electrolytes](#)  
2021. ACS Applied Materials and Interfaces, 13 (18), 21166–21174.  
[doi:10.1021/acsami.1c00366](https://doi.org/10.1021/acsami.1c00366)

Lizenzinformationen: [KITopen-Lizenz](#)